



## **Literature review on crack retrofitting in steel by Tungsten Inert Gas remelting**

Downloaded from: <https://research.chalmers.se>, 2026-04-04 05:54 UTC

Citation for the original published paper (version of record):

al-Karawi, H. (2023). Literature review on crack retrofitting in steel by Tungsten Inert Gas remelting. *Ships and Offshore Structures*, 18(4): 463-468. <http://dx.doi.org/10.1080/17445302.2021.2020986>

N.B. When citing this work, cite the original published paper.

# LES/FGM investigation of ignition and flame structure in a gasoline partially premixed combustion engine

Leilei Xu <sup>a,\*</sup>, Yan Zhang <sup>b,a,\*</sup>, Qinglong Tang <sup>c</sup>, Bengt Johansson <sup>d</sup>,  
Mingfa Yao <sup>b</sup>, Xue-Song Bai <sup>a</sup>

<sup>a</sup> Division of Fluid Mechanics, Lund University, Lund 22100, Sweden

<sup>b</sup> State Key Laboratory of Engines, Tianjin University, Tianjin 300072, PR China

<sup>c</sup> Clean Combustion Research Center, King Abdullah University of Science and Technology, Thuwal, Saudi Arabia

<sup>d</sup> Combustion Engine Research Center (CERC), Chalmers University of Technology, Gothenburg 41296, Sweden

Received 5 January 2022; accepted 25 July 2022

Available online 20 September 2022

## Abstract

This paper presents a joint numerical and experimental study of the ignition process and flame structures in a gasoline partially premixed combustion (PPC) engine. The numerical simulation is based on a five-dimension Flamelet-Generated Manifold (5D-FGM) tabulation approach and large eddy simulation (LES). The spray and combustion process in an optical PPC engine fueled with a primary reference fuel (70% iso-octane, 30% n-heptane by volume) are investigated using the combustion model along with laser diagnostic experiments. Different combustion modes, as well as the dominant chemical species and elementary reactions involved in the PPC engines, are identified and visualized using Chemical Explosive Mode Analysis (CEMA). The results from the LES-FGM model agree well with the experiments regarding the onset of ignition, peak heat release rate and in-cylinder pressure. The LES-FGM model performs even better than a finite-rate chemistry model that integrates the full-set of chemical kinetic mechanism in the simulation, given that the FGM model is computationally more efficient. The results show that the ignition mode plays a dominant role in the entire combustion process. The diffusion flame mode is identified in a thin layer between the ultra fuel-lean unburned mixture and the hot burned gas region that contains combustion intermediates such as CO. The diffusion flame mode contributes to a maximum of 27% of the total heat release in the later stage of combustion, and it becomes vital for the oxidation of relatively fuel-lean mixtures.

© 2022 The Author(s). Published by Elsevier Inc. on behalf of The Combustion Institute.

This is an open access article under the CC BY license (<http://creativecommons.org/licenses/by/4.0/>)

**Keywords:** Partially premixed combustion (PPC); Combustion mode; Flamelet-generated manifold (FGM); Large eddy simulation (LES); Chemical explosive mode analysis (CEMA)

## 1. Introduction

Although electric and hybrid electric vehicles are potential candidates as alternatives to internal

\* Corresponding authors.

E-mail addresses: [leilei.xu@energy.lth.se](mailto:leilei.xu@energy.lth.se) (L. Xu), [zytju@tju.edu.cn](mailto:zytju@tju.edu.cn) (Y. Zhang).

<https://doi.org/10.1016/j.proci.2022.07.214>

1540-7489 © 2022 The Author(s). Published by Elsevier Inc. on behalf of The Combustion Institute. This is an open access article under the CC BY license (<http://creativecommons.org/licenses/by/4.0/>)

combustion engines (ICE), especially in the light-duty vehicle category, ICEs are still expected to remain as the main power source for heavy-duty vehicles, ships, and many machines due to their durability and higher thermal efficiency [1]. However, ICEs are also the primary source of greenhouse gas and pollutant emissions. For further improvement of engine thermal efficiency to meet the ambition of reducing greenhouse gas CO<sub>2</sub> emissions, advanced combustion technologies, e.g., low-temperature combustion (LTC) concepts, including, for example, homogeneous charge compression ignition (HCCI) [2], partially premixed combustion (PPC) [3], and reactivity controlled compression ignition (RCCI) [4], were proposed and comprehensively studied. LTC engines deal with the source of emissions in the combustion chamber by manipulating the stratification of the charge in the cylinder, aiming to simultaneously achieve a low pollutant emission and high efficiency in ICEs. Among these LTC concepts, PPC engines fueled with low-reactivity fuels are a promising and close to commercialization technology, which can be operated at full load with acceptable acoustic noise, high efficiency and low emissions [3].

Although PPC engines have been widely studied in experiments and numerical simulations, most works only focus on engine performance and emissions. Knowledge of the flame structure and reaction front propagation in PPC engines is still limited. In PPC engines, the fuel is injected in the compression stroke before the start of combustion, such that a limited time is available for the fuel/air mixing. As a result, a partially premixed fuel-air mixture is formed with a certain stratification of temperature and equivalence ratio [5]. Auto-ignition in such mixture takes place first in the hot and/or fuel-rich site. Multiple combustion modes are involved inside the combustion chamber, including ignition wave propagation similar to that in HCCI engines, premixed flame propagation similar to that in spark ignition engine and conventional diesel combustion (CDC) in compression ignition engines [6]. To understand the combustion mechanisms in PPC engines, optical diagnostic experiments and numerical simulations were carried out. Tang et al. [7,8] employed optical diagnostic methods to evaluate the ignition and flame development of gasoline PPC. The flame front propagation during the early stages of the flame development process is distinguished using planar laser-induced fluorescence (PLIF) imaging of both formaldehyde (CH<sub>2</sub>O) and hydroxyl (OH) radicals. They reported that multiple auto-ignition kernels emerged in the fuel-rich regions and the reaction front propagates from the auto-ignition kernels towards fuel-lean regions. In the two-dimensional (2D) direct numerical simulation (DNS) work of Luong et al. [9], the budget analysis and Damköhler ( $Da$ ) number based approach were used to distinguish the deflagra-

tion and spontaneous ignition combustion modes during the early phase of combustion in stratified fuel/air mixtures. In the Damköhler-based method, the local  $Da$  is defined based on the ratio of the local chemical and diffusion source terms of selected scalars, and the deflagration mode is identified using the criterion of  $Da < Da_0$ , where  $Da_0$  is a threshold value to be empirically determined. Xu et al. [10] reported that the results of the Damköhler-based method are strongly dependent on the flame configuration or the fuel type and are inconsistent using the different selected scalars and threshold values. Ibron et al. [11] carried out a large eddy simulation (LES) coupled with the partially stirred reactor (PaSR) model to investigate the structures and propagation of the reaction fronts in a PPC engine and found that the transition from auto-ignition to flame occurs over a period of several crank angles.

The onset of multiple combustion modes in PPC engines and its impact on the performance of PPC engines are still not well understood. Both detailed optical engine experiments and high-precision numerical simulations (e.g., LES) are needed to study PPC engines under varied conditions. There are two challenges in numerical simulations of PPC engine combustion under a range of engine conditions. First, a highly computational efficient combustion model is required to properly model the turbulence-chemistry interaction (TCI) and to capture multiple combustion modes in PPC engines. Second, a quantitative analysis approach is needed to distinguish multiple combustion modes in complex engine combustion. This paper presents a new five-dimensional (5D) flamelet-generated manifold (FGM) combustion model. The 5D-FGM model was coupled with LES to study an optical PPC engine combustion process, including spray development, the onset of ignition, and multiple mode combustion. Pressure and PLIF measurements of fuel-tracer were carried out in the optical engine. A Chemical Explosive Mode Analysis (CEMA) method is used to identify the different combustion modes as well as the dominant chemical species and reactions to gain an improved understanding of the mechanisms of ignition and reaction front propagation in the PPC engine. To the best of our knowledge, a detailed LES combined with a CEMA study of the combustion modes in a PPC engine has not been reported. This paper aims to provide new knowledge for understanding the flame development and combustion modes in PPC engines.

## 2. Experimental and numerical setup

### 2.1. Optical engine setup

The experiments were carried out on a single-cylinder optical engine, as shown in Fig. 1. The en-

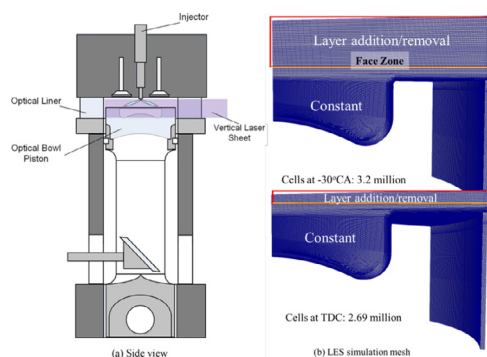


Fig. 1. (a) Schematic of the optical engine experiment setup; (b) LES mesh configuration.

Table 1  
Engine specifications and operating conditions.

Description (units)	Value
Bore/Stroke (mm)	85/90
Connecting rod (mm)	138
Geometric compression ratio	9.5
Swirl ratio	1.5
Intake valve closed ( $^{\circ}$ CA ATDC)	-135
Exhaust valve open ( $^{\circ}$ CA ATDC)	130
Engine speed (r/min)	1200
Intake manifold pressure (bar)	1.5
Injection timing ( $^{\circ}$ CA ATDC)	-30
Engine load (bar)	3.5
Injection pressure (bar)	500
Injection Temperature (K)	348
Injector (mm)	$8 \times 0.18$
Global equivalence ratio	0.28

engine has a bore/stroke length of 85/90 mm with a connecting rod of 138 mm. The engine specifications are given in Table 1. The optical engine utilizes a quartz piston crown and an extended piston sleeve that allows for optical access from the bottom of the piston. A quartz liner with an outer diameter of 135 mm and a height of 29 mm replaces the upper part of the cylinder wall and is clamped onto the bottom surface of the cylinder head by a hydraulic vacuum pump. The vertical laser sheet passes through the quartz liner, and the in-cylinder phenomenon is visible from the side view. An  $\omega$ -shape piston bowl with a raised bottom surface was used, which provided a compression ratio of 9.5:1, cf. Fig. 1(b). The squish height at the top dead center (TDC) is 4 mm. Further detailed engine setup is referred to Ref. [8].

The engine was operated without exhaust gas recirculation (EGR), and the injection timing started from  $-30^{\circ}$  crank angle (CA) after top dead center (ATDC) to achieve an optimal PPC regime [5,8]. Note, in the following, 'CA ATDC' will be abbrevi-

ated to 'CA'. The engine speed was maintained at 1200 rpm. The fuels used were primary reference fuel (PRF70, 70% iso-octane and 30% n-heptane by volume), which is widely used to represent a low octane number gasoline fuel. The intake air was provided by an external compressor, and intake pressure was set to 1.5 bar. The intake air was heated to 348 K by an externally-powered air heater to maintain the CA50 (the crank angle at which 50% of heat was released) at  $5^{\circ}$  CA. The engine was operated at a low load, 3.5 bar IMEP. The common rail supplied the fuel to an eight-hole solenoid injector with a hole diameter of 180  $\mu$ m and an umbrella spray angle of  $162^{\circ}$ . The injection pressure was 500 bar. The injector and injection pressure were selected for the present optical engine to achieve a reasonable injection duration ( $\sim 6^{\circ}$ CA). The total injected fuel mass was 14 mg per cycle. A pressure sensor was used to measure the in-cylinder pressure during the engine combustion process with a resolution of  $0.2^{\circ}$ CA. One hundred continuously fired cycles were recorded, and the last 50 cycles were used to calculate the mean pressure trace. The spray/wall interaction was illustrated using the fuel-tracer (toluene) PLIF imaging, which was carried out under non-reactive conditions by replacing the intake air by pure nitrogen. Toluene of 1% by volume was mixed with the PRF70 fuel and served as the fuel tracer. This minor additive is expected to have a negligible effect on the fuel distribution.

## 2.2. Numerical simulation methodology

### 2.2.1. Numerical model

The simulations were conducted using an in-house solver developed for compressible turbulent flow on the computational fluid dynamics (CFD) platform OpenFOAM-V7 [12]. The fuel spray process was modeled based on the well-established Lagrangian-Eulerian approach. The LES model consists of the spatially filtered continuity equation, transport equations for momentum, and FGM control variables. The sub-grid-scale (SGS) stress and transport fluxes were modeled using a one-equation eddy model [13], based on the transport equation of SGS turbulent kinetic energy. Spray droplets were simulated in the Lagrangian framework and were subject to several processes from the time of injection until the time of vaporisation. The injection profile was described using the model of Xu et al. [14] that was validated and successfully applied for different injection conditions. The time delay between the actual injection of the fuel and the electronic control unit (ECU) signal was  $3^{\circ}$ CA based on the optical engine experiment. The hybrid Kelvin-Helmholtz Rayleigh Taylor (KHRT) model with the recommended model parameters described in Ref. [15] was adopted to predict the liquid droplet breakup process. Droplet collision dynamics was represented using a trajectory-based model in which the probability

of collisions was calculated based on the position and velocity vectors of droplets [16]. The Ranz-Marshall correlation [17] was used to model the fluid-particle heat transfer of droplets in the hot gas flow, while the evaporation was modeled using the Spalding formula [18]. The 'stochasticDispersion-RAS' model [19] was used in this work, where the turbulent velocity is modeled using a Gaussian distribution with variance calculated using the kinetic energy of turbulence. To reduce the computational time, closed-cycle simulations were performed from intake valve close (IVC) (-139.0 °CA) to exhaust valve open (EVO) (130 °CA). For the initial conditions at the IVC, the charge temperature, pressure, and species mass fractions and density were assumed to be uniform in the entire combustion chamber. The initial flow inside the cylinder was assumed to be a solid-body rotational flow with a swirl ratio of 1.5 (in accordance with experiments). The turbulence intensity is assumed to be 0.1 of the average piston velocity. Further details of the spray and LES models used in this study are referred to Refs. [11,20].

### 2.2.2. 5D-FGM combustion model

The FGM combustion model adopted in this study was a tabulated chemistry modeling approach which was based on the flamelet concept [21]. The local thermo-chemical properties were retrieved from representative laminar flames (called flamelets) according to selected FGM control variables. A counterflow diffusion flame configuration was applied to represent the turbulent non-premixed spray combustion. The flame equations were solved in physical space using CHEM1D [22,23]. The governing equations used in CHEM1D are written as,

$$\frac{\partial \rho}{\partial t} + \frac{\partial \rho u}{\partial x} = -\rho K, \quad (1)$$

$$\frac{\partial \rho Y_k}{\partial t} + \frac{\partial \rho u Y_k}{\partial x} = \frac{\partial}{\partial x} \left( \rho D \frac{\partial Y_k}{\partial x} \right) + \dot{\omega}_k - \rho K Y_k, \quad (2)$$

$$\frac{\partial \rho h}{\partial t} + \frac{\partial \rho u h}{\partial x} = \frac{\partial}{\partial x} \left( \frac{\lambda}{C_p} \frac{\partial h}{\partial x} \right) - \rho K h. \quad (3)$$

where the local flame stretch rate,  $K = \partial v / \partial y$ , represents the flow effect on flame. The conservation equation of  $K$  is solved by:

$$\frac{\partial \rho K}{\partial t} + \frac{\partial \rho u K}{\partial x} = \frac{\partial}{\partial x} \left( \mu \frac{\partial K}{\partial x} \right) + \rho_{ox} a^2 - \rho K^2, \quad (4)$$

where  $\rho_{ox}$  and  $a$  are the density and the prescribed strain rate in the oxidizer stream, respectively. To minimize the FGM dimension the strain rate is not considered as a variable. The strain rate of 200 1/s is representative of the present case, and this value is kept the same for all chem1D simulations [24]. Detailed discussion on the flamelet solution method in CHEM1D can be found in Refs. [22,23].

The control variables in the FGM model are the mixture fraction of the PRF70 fuel  $\tilde{Z}$ , the normalized progress variable  $\tilde{C}$ , the absolute enthalpy on the oxygen side  $\tilde{h}_0$  and the pressure  $\tilde{p}$ . Here, quantities with bar indicate spatially filtered, while with tilde they are density-weighted spatially filtered. This model is referred to as 4D-FGM, since it involves four control variables. To consider the different evaporation rates of the two fuels in the PRF fuel mixture, another control variable,  $\tilde{Z}_2$ , which is the local mass fraction of n-heptane, was introduced. Since n-heptane evaporates faster than iso-octane, the volume ratio of the two fuels varies in space as will be discussed later. This spatially varying IC8H18/C7H16 volume ratio has a significant impact on the low-temperature ignition process, and it has been neglected in the previous FGM literature [25]. The mixture fraction is calculated using Bilger's formula [26]. The progress variable is defined following the recent work of Lucchini et al. [24],  $Y_c = 2.7Y_{\text{HO}_2} + 1.5Y_{\text{CH}_2\text{O}} + 0.9Y_{\text{CO}} + 1.2Y_{\text{H}_2\text{O}} + 1.2Y_{\text{CO}_2}$ . The transported  $\tilde{Y}_c$  needs to be normalized to  $\tilde{C}$ :

$$\tilde{C} = \frac{\tilde{Y}_c - \tilde{Y}_c^u(\tilde{Z}, \tilde{Z}_2, \tilde{h}_0, \tilde{p})}{\tilde{Y}_c^b(\tilde{Z}, \tilde{Z}_2, \tilde{h}_0, \tilde{p}) - \tilde{Y}_c^u(\tilde{Z}, \tilde{Z}_2, \tilde{h}_0, \tilde{p})}, \quad (5)$$

where  $\tilde{Y}_c^u$  and  $\tilde{Y}_c^b$  are the minimum and maximum progress values, respectively. Finally, five control variables are stored in the 5D-FGM tables indexed by  $\tilde{C}$ ,  $\tilde{Z}$ ,  $\tilde{Z}_2$ ,  $\tilde{h}_0$  and  $\tilde{p}$ .

A skeletal reaction mechanism for iso-octane and n-heptane [27], including the extended Zeldovich mechanism for Nitrogen Oxides ( $\text{NO}_x$ ) prediction, was used to generate the flamelet libraries in CHEM1D simulations. The mechanism consists of 136 species and 617 elementary reactions, which has been extensively validated against experimental data, including ignition delay times measured in the shock tube, species mole fraction profiles in Jet-Stirred Reactor, and laminar flame speeds. The PaSR model [16,28] was also used as a reference model to compare with the newly developed FGM model. In the PaSR model, the spatially filtered reaction rates are computed similarly to the well-stirred reactor (WSR) model but scaled according to a factor,  $\kappa = \tau_c / (\tau_c + C_{\text{mix}} \tau_t)$ , where  $\tau_c$  and  $\tau_t$  are a chemical and turbulent timescale, respectively.  $C_{\text{mix}}$  is set to 0.1, following our previous work [11]. The turbulent timescale,  $\tau_t$ , is estimated by the geometrical mean of integral and Kolmogorov time scales,  $\tau_t = (k/\epsilon)^{1/2} (\nu/\epsilon)^{1/4}$ , where  $k$ ,  $\epsilon$ , and  $\nu$  are the turbulent kinetic energy, dissipation rate, and kinematic viscosity, respectively. The chemical timescale is calculated based on the formation/consumption rates of major species, e.g., fuel or oxidizer. To speed up the simulation, the chemical reaction rates of the PaSR model are integrated into the transport equations using a speed-up algorithm, the chemistry coordinate mapping (CCM) method [29], in which the calculations of re-

action rates are performed for groups of cells. The grouping is based on a chemistry phase space made up of five dimensions, equivalence ratio, scalar dissipation rate, temperature, and mass fractions of nitrogen and fuels (iso-octane and n-heptane). The equivalence ratio in the CCM method is calculated based on the elements of C, H, O,  $\Phi = (2X_C + 0.5X_H)/X_O$ , where,  $X$  is the element mole fraction [5].

### 2.2.3. Dynamic mesh algorithm

The computational domain is a 45° sector of the full cylinder, representing one spray plume. To maintain the mesh quality (size and shape of cells) and mesh density throughout the simulation of the entire engine strokes, a dynamic mesh layer algorithm [30] was developed based on OpenFOAM, which incorporates the adding and removing of cells in accordance with the motion of the engine piston. A face zone layer (1 mm offset above the piston crown, cf. Fig. 1(b)) was selected to distinguish between the dynamic and constant cell domains, cf. Fig. 1(b). Cells below the selected face zone remained unchanged during the simulation. The layer thickness above the selected face zone was continuously monitored during the simulation: a layer of cells was added during the expansion stroke when the thickness of the stretched layer increased above a specified threshold (0.2 mm in this study) and cells were removed/merged into neighboring cells above during the compression stroke when the deforming layer thickness decreased below a threshold (0.08 mm), cf. Fig. 1(b). A mesh sensitive study was conducted in our previous work, with similar piston shape and engine operation conditions [11]. The results showed that the 0.20 mm grid size resolution could yield a good prediction of the spray and combustion process with affordable computational efficiency.

## 3. Results and discussion

### 3.1. Comparison of LES results with experiments

Validation of the simulation results was performed by comparing the in-cylinder pressure trace, and apparent heat release rate (AHRR) obtained from the experiment and the LES using the different combustion models, i.e., PaSR, 4D-FGM, and 5D-FGM, with the same initial and boundary conditions. As shown in Fig. 2, after the fuel is injected into the cylinder, two heat-release stages can be found from the AHRR profile. The low-temperature ignition stage occurs in the crank angle range of  $-20 \sim -15^\circ\text{CA}$ . The high-temperature ignition stage starts slightly before the TDC, followed by a rapid heat release and pressure rise. With the same initial and boundary conditions, the 5D-FGM and PaSR models yielded similar results, while the 4D-FGM model predicted a

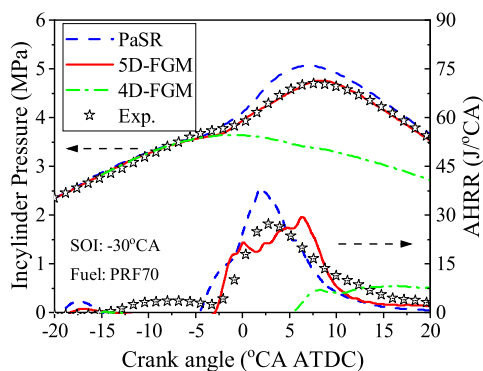


Fig. 2. In-cylinder pressure and apparent heat release rate (AHRR) from the simulations and experiments.

very late ignition and poor combustion efficiency. Compared with the experimental results, the results from the 5D-FGM model showed better agreement with the experiments in terms of the onset of high-temperature ignition, in-cylinder pressure and peak AHRR. The PaSR model predicted an earlier ignition and higher peak AHRR, resulting in a larger peak value of cylinder pressure. The parameters of the PaSR model (i.e. the model constant  $C_{mix}$ ) may be tuned to achieve a better prediction; in general, the PaSR model with a larger  $C_{mix}$  yields a slower heat release rate and later ignition. The PaSR results are then expected to agree better with the experiments. Such tuning is not attempted here since the model is used here as a reference for comparison with the FGM models in terms of computational efficiency. In the PaSR model, the transport equations for the entire species in the mixture are solved (135 species transport equations), which is time-consuming. The FGM model solves five transport equations for the control variables; thus, the computational time required in the FGM model is significantly lower than that in the PaSR model. The computational time of the present 5D-FGM model is about 10% of that required by the PaSR model.

In PPC engines, the fuel is typically injected at an early SOI ( $-30^\circ\text{CA}$  in this study) and the liquid penetration of fuel spray is long due to the low ambient pressure, low temperature and low density of the ambient gas in the cylinder. To explore the temporal evolution of the vapor fuel distribution in the cylinder, Fig. 3 shows the instantaneous distribution of mixture fraction of the PRF70 fuel ( $Z$ ) predicted by the LES-FGM and LES-PaSR models, along with the cycle-averaged fuel tracer PLIF intensity (from 30 consecutive engine cycles). The fuel was injected into the squish region towards the piston crown. The fuel is deflected on the piston crown and flows towards the crevice, and then to the cylinder head, and finally to the piston bowl; owing to the piston squishing motion, the fuel is

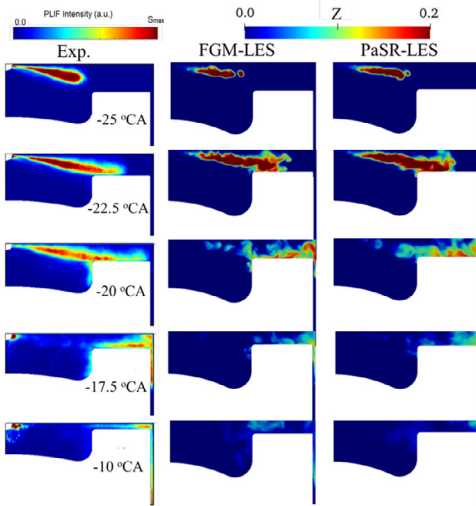


Fig. 3. Fuel-tracer PLIF intensity (arbitrary unit, a.u.) and LES predicted mixture fraction.

being transported from the squish region into the piston bowl. At  $-10^\circ\text{CA}$ , a pocket of the fuel-lean mixture is formed in the bowl region due to the recirculating flow motion. The fuel in the crevice and squish regions is difficult to mix with the air due to the confinement of the piston and cylinder walls. As a result, a relatively fuel-rich mixture is formed in the crevice and the squish regions. From the comparison of the fuel distribution in the experimental measurements and simulations, LES-FGM and LES-PaSR models both can qualitatively well predict the development of the spray and the spray/wall interaction. The main difference between the LES results and the PLIF experiments may be due to that the PLIF intensity was cycle-averaged one while the LES results are single cycle results (which is intended to show the temporal evolution of the vapor fuel distribution). Also, the uncertainty of the injection rate and spray models may contribute to certain difference in the results.

Due to the different evaporation rates of iso-octane and n-heptane, the local ratio of the volume fraction of the two fuels (the PRF number) is different from that in the liquid form (PRF70). As shown in Fig. 4, the n-heptane evaporates faster than the iso-octane, and the local PRF number can be as low as 65 (35% n-heptane by volume), which will result in an earlier ignition timing. In the 5D-FGM, the difference in the evaporation rate is modeled by the spray model and quantified using two mixture fractions  $Z$  and  $Z_2$ , while in the 4D-FGM model, only one mixture fraction  $Z$  (for the total PRF70 fuel) was solved and the fuel ratio in the local cell is the same as that in the liquid form. Thus, compared with the 5D-FGM and PaSR model, the conventional 4D-FGM model predicts a much later ignition timing and subsequently poor combustion efficiency, cf. Fig. 2.

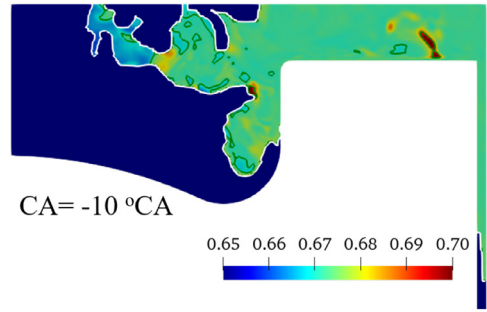


Fig. 4. Distribution of local iso-octane and n-heptane volume ratio in the cylinder at  $\text{CA} = -10^\circ\text{CA}$ , simulated using the 5D-FGM LES model.

### 3.2. Identification of combustion mode

The PPC engine regime is characterized by the mixture with equivalence ratio stratification in the cylinder ranging from fuel-rich ( $\Phi > 1.2$ ) to fuel-lean ( $\Phi < 0.8$ ) at the CAD of onset of ignition [31]. In such mixture, there exists multiple combustion modes, ignition wave propagation or premixed flame propagation in the fuel-rich and fuel-lean mixtures, and diffusion flame around the stoichiometric mixture [32]. It is critical to identify the different combustion modes in order to develop control strategies of the combustion process. A more systematic approach, chemical explosive mode analysis (CEMA) is applied here to identify the combustion modes. CEMA was originally developed by Lu et al. [33] as a systematic diagnostic tool of identifying critical flame features, and has been applied to different types of complex turbulence flames to identify premixed reaction fronts, mixtures undergoing auto-ignition and local extinction, and cool flames, etc. [10,34,35]. CEMA is based on an eigen-analysis of the local chemical Jacobian matrix,

$$\frac{D\omega(\mathbf{y})}{Dt} = \mathbf{J}_\omega \frac{D\mathbf{y}}{Dt} = \mathbf{J}_\omega(\omega + \mathbf{s}), \quad (6)$$

where  $\mathbf{J}_\omega = \partial\omega/\partial\mathbf{y}$  is the local chemical Jacobian matrix.  $\mathbf{y}$  is the vector of local dependent variables including temperature and species mass fractions.  $\omega$  is the chemical source term, and  $\mathbf{s}$  is the non-chemical source term, such as the diffusion term. An eigenvalue,  $\lambda_e$ , which has a positive real part, is used to identify the chemical explosive mode (CEM) [33].

A new criterion proposed by Xu et al. [10] was used to distinguish the different combustion modes. Eq. (6) is projected in the direction of the corresponding eigenvectors,  $\mathbf{b}_e$ , of  $\mathbf{J}_\omega$ ,

$$\mathbf{b}_e \cdot \frac{D\omega(\mathbf{y})}{Dt} = \mathbf{b}_e \cdot \mathbf{J}_\omega(\omega + \mathbf{s}) = \lambda_e \mathbf{b}_e \cdot (\omega + \mathbf{s}), \quad (7)$$

$$\frac{D\phi_\omega}{Dt} = \lambda_e \phi_\omega + \lambda_e \phi_s + \frac{D\mathbf{b}_e}{Dt} \cdot \omega(\mathbf{y}) \quad (8)$$

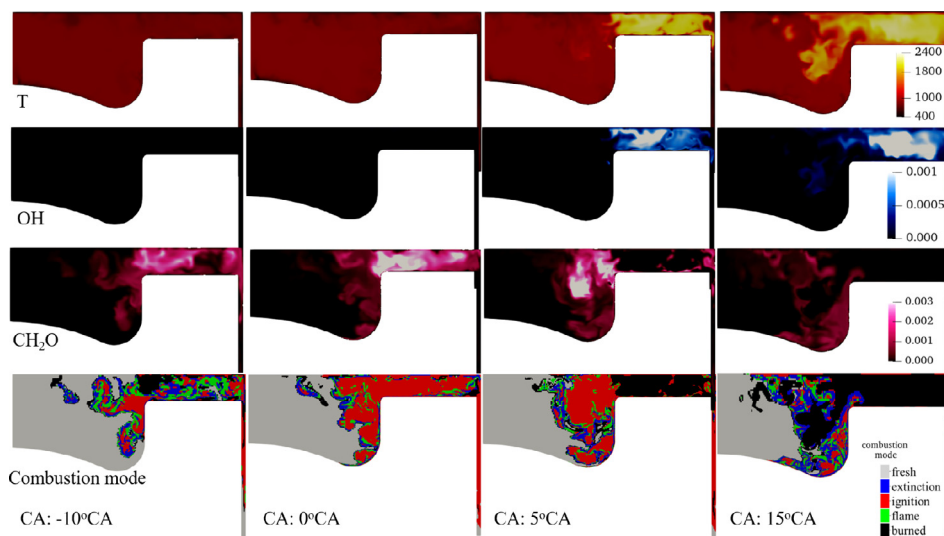


Fig. 5. Spatial distribution of temperature, mass fractions of OH and  $\text{CH}_2\text{O}$  and local combustion modes identified by CEMA.

Table 2  
Local combustion modes distinguished by CEMA.

criterion	$\alpha < -1$	$-1 < \alpha < 1$	$1 < \alpha$
$\lambda_e < 0$	burned	burned	burned
$0 < \lambda_e < 1$	fresh	fresh	fresh
$\lambda_e > 1$	extinction	ignition	flame

where the projected chemical ( $\phi_\omega \equiv \mathbf{b}_e \cdot \omega$ ) and diffusion ( $\phi_s \equiv \mathbf{b}_e \cdot \mathbf{s}$ ) source terms are used to calculate a local combustion mode indicator,  $\alpha = \phi_s / \phi_\omega$ . The local combustion modes identified using CEMA are listed in Table 2, where "burned", "fresh", "ignition", "flame" and "extinction" indicate respectively that the local mixture is at burned gas mode, fresh reactant mode, ignition mode, flame mode, and extinction mode. Note that here for convenience the "burned" and "fresh" are referred to as two "combustion" modes since they can be identified using CEMA. Further details of the CEMA are referred to the Refs. [10,33,36] and references therein.

Fig. 5 shows the instantaneous distributions of temperature and mass fractions of OH,  $\text{CH}_2\text{O}$ , and local combustion modes (identified using CEMA) on the middle plane at different crank angles. At  $-10^\circ\text{CA}$ , a significant amount of  $\text{CH}_2\text{O}$  was already formed in the squish region. With the piston moving upward, the mixture temperature increases, and more  $\text{CH}_2\text{O}$  is produced and accumulated in the squish region. The temperature is still low and no OH radicals could be identified. In the  $\text{CH}_2\text{O}$  region, one can see multiple combustion modes, including chemically inert modes (burned region), ignition, extinction, and flame regions. The ignition

is at its first stage (low-temperature ignition stage) and the flame is in a cool flame mode. The "burned" region indicates where the first-stage ignition has ended and  $\text{CH}_2\text{O}$  has ended its production. Later at TDC in Fig. 5, there are still no obvious OH radicals on the shown cross-section plane; the first stage ignition mode is the dominant mode in the combustion chamber, and the cool flame mode can also be identified in a thin layer surrounding the ignition mode region. At the CA50 ( $5^\circ\text{CA}$ ), large amounts of OH radicals are already formed in the squish region where  $\text{CH}_2\text{O}$  is oxidized. Fuel in the squish region is almost completely oxidized and the mixture is therefore at the burned gas mode. In the piston bowl, a large region is in the first-stage ignition mode which results in the formation of  $\text{CH}_2\text{O}$ . The boundary of the ignition region shows a mix of cool flame propagation mode, extinction and burned gas modes. At  $15^\circ\text{CA}$ , most fuel is burned and a large region remained unburned fresh mixture due to little fuel mixed with the air. In the boundary of the burned gas and unburned gas, combustion is at the flame mode. Since the unburned mixture in the high-temperature region mixes with the low-temperature air-rich region, and combustion is a mixing controlled, thus at the diffusion flame mode. In the region near the wall of the piston bowl, a mix of cool flame propagation and first-stage ignition modes can be identified.

CEMA can be used to identify critical variables and reactions of important species, i.e., using the explosive index (EI) of the variables and the participation index (PI) of the reactions. The definition of EI and PI is referred to Refs. [33,37]. The EI of temperature and all species mass fractions, and the

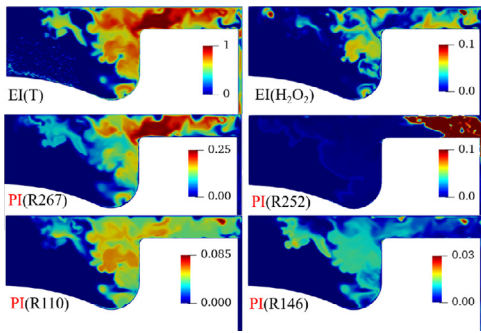


Fig. 6. Spatial distribution of EI and PI of important variables and reactions at the ignition stage ( $1^\circ\text{CA}$ ).

PI of all reactions are computed from CEMA. The first two key variables that have the highest EI and the four reactions that have the highest PI are identified. The spatial distribution of EI of the two key variables and PI of the four key reactions at  $1^\circ\text{CA}$  are shown in Fig. 6. As already shown in Figs. 2 and 5, at  $1^\circ\text{CA}$  the dominant mode of combustion is the ignition mode. The most important variable at this ignition stage is temperature, which indicates the thermal runaway process. Besides,  $\text{H}_2\text{O}_2$  is the most important species whose decomposition to form OH radicals results in a radical runaway process. As the temperature is increased above 1000 K,  $\text{H}_2\text{O}_2$  decomposition exceeds its production, and the resulting pool of OH radicals accelerates the overall rate of oxidation, leading to the rapid heat release [6]. Fig. 6 shows that the reaction that has the highest PI is the chain branching reaction R267 ( $\text{H}_2\text{O}_2 \rightleftharpoons 2\text{OH}$ ), which is the main source of production of OH radicals. The key role of this reaction in promoting ignition has been identified in the oxidation of a variety of hydrocarbon fuels, i.e.,  $\text{CH}_4$ , DME, iso-octane, etc. [38]. The chain-branching reaction R252 ( $\text{H} + \text{O}_2 \rightleftharpoons \text{O} + \text{OH}$ ) is identified as another most important elementary reaction in the high-temperature reaction stage. Through this reaction, accumulated H radicals are rapidly consumed producing O and OH radicals. In addition, R110 ( $\text{C}_3\text{H}_5 + \text{HO}_2 \rightleftharpoons \text{OH} + \text{C}_2\text{H}_3 + \text{CH}_2\text{O}$ ) and R146 ( $\text{C}_2\text{H}_4 + \text{OH} \rightleftharpoons \text{C}_2\text{H}_3 + \text{H}_2\text{O}$ ) are also found to be important for ignition. It appears that a large amount of intermediate species is produced in the low-temperature reaction stage, increasing the reactivity of the mixture. The final oxidation of these intermediate species plays an important role in the high-temperature ignition process.

To quantify the contribution of ignition and flame modes to the combustion heat release, the total heat release rate (HRR) in the cylinder from each mode was calculated based on the CEMA results. The total HRR and the fraction of HRR that comes from the ignition and the flame modes are identified and plotted in Fig. 7. From the to-

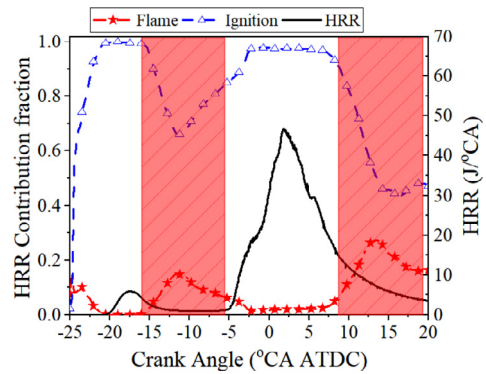


Fig. 7. Contribution of the different combustion modes to the total heat release rate in the PPC engine.

tal HRR profile one can identify two-stage heat release: the first stage heat release (low temperature ignition, from  $-20^\circ\text{CA}$  to  $-10^\circ\text{CA}$ ), and the main combustion heat release (after  $-5^\circ\text{CA}$ ). It can be seen that the ignition mode is the dominant one contributing to the heat release during the entire combustion process. Around the two peak HRR, nearly the entire heat release is from the ignition mode combustion. The cool flame mode is relatively important in the later first stage heat release (from  $-15^\circ\text{CA}$  to  $-10^\circ\text{CA}$ ). Note that during the cool flame propagation (corresponding to the propagation of the  $\text{CH}_2\text{O}$  region in Fig. 5), the HRR is rather low. The flame mode is relatively important in the later stage combustion, after  $5^\circ\text{CA}$ , contributing to a maximum of 27% of the total heat release. From Fig. 5, it is understood that diffusion flame is the dominant mode that occurs at the boundary between the burned gas region and fresh reactant region, where combustion is controlled by the diffusion of the oxidizer from the fresh air-rich gas and diffusion of combustion intermediate from the burned region.

In the later stage of combustion, there is a large region that is identified as a fresh gas region, Fig. 5. In this region, the mixture is ultra fuel-lean. Combustion of the lean mixture is important for the reduction of unburned fuel and CO emissions in the engine. Since the flame mode is important in the later stage combustion it is expected that increasing in-cylinder turbulence, which can enhance the turbulent diffusion of the unburned fuel/combustion intermediate in the 'burned' region and the air-rich fresh gas to the diffusion flame region, will help reduce the emissions.

#### 4. Conclusion

LES coupled with a new FGM model was performed to investigate the combustion process in an optical PPC engine fueled with PRF70 fuel.

The LES-FGM model was validated by comparison with the optical engine experiment and the LES-PaSR model. The different flame modes, key variables, and reactions involved in the PPC engine are identified using CEMA. The following conclusions are drawn:

- The LES-FGM model can well capture the main combustion characteristics in PPC engines, with good agreement with experiments in terms of the start of high-temperature ignition, in-cylinder pressure profile, and peak AHRR. The LES-FGM model can give an even better prediction of these combustion characteristics than the often used finite-rate chemistry model based on PaSR, which is based on direct integration of the full chemical kinetic mechanism, given that the computational cost of LES-FGM is significantly lower than the finite-rate chemistry model.
- The multiple combustion modes in the PPC engines were visualized with CEMA, along with the identification of the dominant chemical species and reactions. The ignition mode is a dominant one contributing to the total heat release rate during the entire combustion process. At the low-temperature ignition stage, cool flame propagation contributes to a small fraction of the total heat release as well. After the high-temperature ignition stage, the diffusion flame mode is an important one in a thin layer between the burned gas region and the fresh reactant region. The emission of unburned fuel and CO is largely governed by the turbulent mixing rate to this thin layer.

#### Declaration of Competing Interest

The authors declare that they have no known competing financial interests or personal relationships that could have appeared to influence the work reported in this paper.

#### Acknowledgments

This work was supported by the Swedish Research Council (VR) and Swedish Energy Agency (STEM) through Competence Centre for the Combustion Processes (KCFP) at Lund University, and the Natural Science Foundation of China (51921004). The simulations were performed on resources provided by the Swedish National Infrastructure for Computing (SNIC). Dr Yan Zhang is sponsored by China Scholarship Council. Our deepest gratitude goes to Prof. Tianfeng Lu and Mr Ji-Woong Park at the University of Connecticut for sharing the CEMA code.

#### References

- [1] G. Kalghatgi, Is it really the end of internal combustion engines and petroleum in transport? *Appl. Energy* 225 (2018) 965–974.
- [2] X. Lu, D. Han, Z. Huang, Fuel design and management for the control of advanced compression-ignition combustion modes, *Prog. Energy Combust. Sci.* 37 (6) (2011) 741–783.
- [3] V. Manente, B. Johansson, W. Cannella, Gasoline partially premixed combustion, the future of internal combustion engines? *Int. J. Engine Res.* 12 (3) (2011) 194–208.
- [4] R.D. Reitz, G. Duraisamy, Review of high efficiency and clean reactivity controlled compression ignition (RCCI) combustion in internal combustion engines, *Prog. Energy Combust. Sci.* 46 (2015) 12–71.
- [5] L. Xu, X.-S. Bai, C. Li, P. Tunestål, M. Tunér, X. Lu, Combustion characteristics of gasoline DICI engine in the transition from HCCI to PPC: experiment and numerical analysis, *Energy* 185 (2019) 922–937.
- [6] M.P. Musculus, P.C. Miles, L.M. Pickett, Conceptual models for partially premixed low-temperature diesel combustion, *Prog. Energy Combust. Sci.* 39 (2–3) (2013) 246–283.
- [7] Q. Tang, H. Liu, M. Li, M. Yao, Z. Li, Study on ignition and flame development in gasoline partially premixed combustion using multiple optical diagnostics, *Combust. Flame* 177 (2017) 98–108.
- [8] V. Raman, Q. Tang, Y. An, H. Shi, P. Sharma, G. Magnotti, J. Chang, B. Johansson, Impact of spray-wall interaction on the in-cylinder spatial unburned hydrocarbon distribution of a gasoline partially premixed combustion engine, *Combust. Flame* 215 (2020) 157–168.
- [9] M.B. Luong, R. Sankaran, G.H. Yu, S.H. Chung, C.S. Yoo, On the effect of injection timing on the ignition of lean prf/air/egr mixtures under direct dual fuel stratification conditions, *Combust. Flame* 183 (2017) 309–321.
- [10] C. Xu, J.-W. Park, C.S. Yoo, J.H. Chen, T. Lu, Identification of premixed flame propagation modes using chemical explosive mode analysis, *Proc. Combust. Inst.* 37 (2) (2019) 2407–2415.
- [11] C. Ibrón, H. Fatehi, Z. Wang, et al, Numerical simulation of a mixed-mode reaction front in a PPC engine, *Proc. Combust. Inst.* 38 (4) (2021) 5703–5711.
- [12] H. Jasak, A. Jemcov, Z. Tukovic, et al., Openfoam: A c++ library for complex physics simulations, in: Proceedings of the International workshop on coupled methods in numerical dynamics, volume 1000, IUC Dubrovnik Croatia, 2007.
- [13] W.-W. Kim, S. Menon, A new dynamic one-equation subgrid-scale model for large eddy simulations, in: Proceedings of the 33rd Aerospace Sciences Meeting and Exhibit, 1995, p. 356.
- [14] L. Xu, X.-S. Bai, M. Jia, Y. Qian, X. Qiao, X. Lu, Experimental and modeling study of liquid fuel injection and combustion in diesel engines with a common rail injection system, *Appl. Energy* 230 (2018) 287–304.
- [15] J.C. Beale, R.D. Reitz, Modeling spray atomization with the Kelvin-Helmholtz/Rayleigh-Taylor hybrid model, *At. Sprays* 9 (6) (1999).
- [16] P. Nordin, Complex Chemistry Modeling of Diesel Spray Combustion, Chalmers University of Technology, 2001. PhD thesis

- [17] W. Ranz, W. Marshall, et al., Evaporation from drops: part 2, *Chem. Eng. Prog.* 48 (4) (1952) 173–180.
- [18] D.B. Spalding, The combustion of liquid fuels, *Proc. Combust. Inst.* 4 (1953) 847–864.
- [19] A. Gosman, E. Loannides, Aspects of computer simulation of liquid-fueled combustors, *J. Energy* 7 (6) (1983) 482–490.
- [20] M. Pucilowski, M. Jangi, H. Fatehi, K.M. Pang, X.-S. Bai, Les study of diesel flame/wall interaction and mixing mechanisms at different wall distances, *Proc. Combust. Inst.* 38 (4) (2021) 5597–5604.
- [21] J. Van Oijen, A. Donini, R. Bastiaans, et al, State-of-the-art in premixed combustion modeling using flamelet generated manifolds, *Prog. Energy Combust. Sci.* 57 (2016) 30–74.
- [22] L.M. Somers, The Simulation of Flat Flames with Detailed and Reduced Chemical Models, Technische Universiteit Eindhoven, 1994. PhD thesis
- [23] C. Bekdemir, Tabulated Chemical Kinetics for Efficient and Detailed Simulations of Diesel Engine Combustion, Technische Universiteit Eindhoven, 2012. PhD thesis
- [24] T. Lucchini, D. Pontoni, G. D’Errico, B. Somers, Modeling diesel combustion with tabulated kinetics and different flame structure assumptions based on flamelet approach, *Int. J. Engine Res.* 21 (1) (2020) 89–100.
- [25] Q. Zhou, T. Lucchini, G. D’Errico, R. Novella, J.M. García-Oliver, X. Lu, CFD Analysis of combustion and emission characteristics of primary reference fuels: from transient diesel spray to heavy-duty engine, *Fuel* 301 (2021) 120994.
- [26] R. Bilger, S. Stårner, R. Kee, On reduced mechanisms for methane-air combustion in nonpremixed flames, *Combust. Flame* 80 (2) (1990) 135–149.
- [27] X. Liu, H. Wang, L. Wei, J. Liu, R.D. Reitz, M. Yao, Development of a reduced toluene reference fuel (TRF)-2, 5-dimethylfuran-polycyclic aromatic hydrocarbon (PAH) mechanism for engine applications, *Combust. Flame* 165 (2016) 453–465.
- [28] Z. Li, M. Ferrarotti, A. Cuoci, A. Parente, Finite-rate chemistry modelling of non-conventional combustion regimes using a partially-Stirred reactor closure: combustion model formulation and implementation details, *Appl. Energy* 225 (2018) 637–655.
- [29] M. Jangi, X.-S. Bai, Multidimensional chemistry coordinate mapping approach for combustion modelling with finite-rate chemistry, *Combust. Theory Model* 16 (6) (2012) 1109–1132.
- [30] T. Lucchini, G. D’Errico, H. Jasak, Z. Tukovic, Automatic mesh motion with topological changes for engine simulation, *SAE 2007-01-0170* (2007).
- [31] L. Xu, X.-S. Bai, Y. Li, et al, Effect of piston bowl geometry and compression ratio on in-cylinder combustion and engine performance in a gasoline direct-injection compression ignition engine under different injection conditions, *Appl. Energy* 280 (2020) 115920.
- [32] F. Zhang, R. Yu, X.-S. Bai, Direct numerical simulation of prf70/air partially premixed combustion under ic engine conditions, *Proc. Combust. Inst.* 35 (3) (2015) 2975–2982.
- [33] T. Lu, C.S. Yoo, J. Chen, C.K. Law, Three-dimensional direct numerical simulation of a turbulent lifted hydrogen jet flame in heated coflow: a chemical explosive mode analysis, *J. Fluid Mech.* 652 (2010) 45–64.
- [34] N.A.K. Doan, S. Bansode, K. Osawa, Y. Minamoto, T. Lu, J. Chen, N. Swaminathan, Identification of combustion mode under mild conditions using chemical explosive mode analysis, *Proc. Combust. Inst.* 38 (4) (2021) 5415–5422.
- [35] C. Xu, M.M. Ameen, S. Som, J.H. Chen, Z. Ren, T. Lu, Dynamic adaptive combustion modeling of spray flames based on chemical explosive mode analysis, *Combust. Flame* 195 (2018) 30–39.
- [36] Y. Zhang, S. Xu, S. Zhong, X.-S. Bai, H. Wang, M. Yao, Large eddy simulation of spray combustion using flamelet generated manifolds combined with artificial neural networks, *Energy AI* 2 (2020) 100021.
- [37] Z. Luo, C.S. Yoo, E.S. Richardson, J.H. Chen, C.K. Law, T. Lu, Chemical explosive mode analysis for a turbulent lifted ethylene jet flame in highly-heated coflow, *Combust. Flame* 159 (1) (2012) 265–274.
- [38] E.-A. Tingas, Z. Wang, S.M. Sarathy, H.G. Im, D.A. Goussis, Chemical kinetic insights into the ignition dynamics of n-hexane, *Combust. Flame* 188 (2018) 28–40.